Proceedings of the IASS 2024 Symposium
Redefining the Art of Structural Design
August 26-30, 2024, Zurich, Switzerland
Philippe Block, Giulia Boller, Catherine DeWolf,
Jacqueline Pauli, Walter Kaufmann (eds.)

Isogeometric smoothed finite element analysis: Numerical investigations on applying essential boundary conditions

Malik QDEIMAT*, Markus KLASSEN[a], Martin TRAUTZ, Sven KLINKEL[b]

* Chair of Structures and Structural Design (Trako), RWTH Aachen University
Schinkelstr. 1, 52062 Aachen, Germany
qdeimat@trako.arch.rwth-aachen.de

[a] CPI Vertex Antennentechnik GmbH, Duisburg
[b] Chair of Structural Analysis and Dynamics (LBB), RWTH Aachen University

Abstract

The Isogeometric Analysis (IGA) approach, developed to smoothly integrate precise geometric descriptions from Computer-Aided Design into numerical solution algorithms of the Finite Element Method (FEM), presents a significant step in structural engineering and architecture. Due to the common use of Non-Uniform Rational B-Splines as basis functions in IGA, there is a dependence on Gauss quadrature integration, often leading to computational expenses during stiffness matrix calculation and postprocessing. Meanwhile, the smoothed finite element method introduces a strain smoothing technique to address issues within FEM, involving a volume-average of strain within specified smoothing domains created on the top of the mesh elements. This paper proposes an innovative approach by merging the strain smoothing technique with IGA, resulting in the Isogeometric Smoothed Analysis. Its main focus centers on generating smoothing domains in the parameter space rather than the physical space. Following this, the method maps physical quantities necessary for implementing the strain smoothing technique from quantities calculated in the parameter space. To achieve this mapping, constructing the Jacobian matrix at the center point of the smoothing domain becomes essential, facilitating the relationship between the two spaces. The numerical findings illustrate that the proposed formulation can deliver accurate solutions with improved convergence rates, particularly in specific cases. This study plays a key part in merging structural engineering and architecture, improving the conversion of complex geometric designs into strong numerical solutions through more efficient methods.Future exploration in this domain may encompass the application of these techniques to diverse element shapes, extension of methodologies to address three-dimensional challenges, and refinement of approaches for improved computational efficiency and accuracy.

Keywords: isogeometric analysis, finite element method, smoothed finite element method, strain smoothing technique, cell-based model, edge-based model, node-based model.

1. Introduction

The Finite Element Method (FEM) is a powerful numerical technique for solving discrete problems represented by partial differential equations (PDEs). It was developed through collaborative efforts of mathematicians and engineers during the 19th and 20th centuries and significantly shaped during the 1950s-1970s with the birth of digital computers. FEM is widely used in structural mechanics, aeronautical, and mechanical engineering [1, 2].

Researchers have extensively studied the properties of FEM, identifying drawbacks outlined in litera-

ture [2, 3, 4]. Standard FEM methods encounter several limitations. Firstly, discretizing geometry into multiple elements introduces significant approximation errors in the solution field. Additionally, elements often display excessive stiffness, leading to accuracy issues and volumetric locking. Moreover, mesh distortion can compromise accuracy and result in poorly conditioned Jacobian matrices. Furthermore, FEM solutions offer only a lower bound, complicating the certification of solutions. Finally, stress solutions suffer from inaccuracies due to stiffness and strain evaluation across element interfaces.

Hughes et al. [5, 6] introduced Isogeometric Analysis (IGA) as an innovative numerical scheme aimed at minimizing geometric errors. IGA employs Non-Uniform Rational B-Splines (NURBS) basis functions for precise geometry representation, maintaining the isoparametric concept of using the same basis functions for both geometry description and solution field, similar to FEM. Studies have demonstrated that IGA yields more accurate and efficient solutions compared to FEM. In a parallel line, Liu et al. [2, 4] proposed integrating the strain smoothing technique into FEM to improve solution accuracy. This led to the development of smoothed finite element methods (S-FEM), which adjust the compatible strain field by introducing various smoothing domains over the element mesh. Common S-FEM models include cell-based (CS-FEM), node-based (NS-FEM), and edge-based (ES-FEM). Recent studies show that these methods effectively address FEM's limitations.

This study aims to explore the application of strain smoothing techniques to IGA, inspired by Liu's work on employing such techniques in FE settings and proposing S-FEM models.The three techniques from S-FEM models will be incorporated into IGA and verified through designated benchmark numerical examples. The implementation of NURBS in IGA guarantees precise geometry representation regardless of mesh refinement. However, NURBS often extend across multiple elements, leading to inefficient Gauss quadrature integration for stiffness matrix calculation. The motivation for this study is many-sided. Firstly, NURBS are recursively defined, requiring extensive calculations to determine the polynomial degree, which results in significant computational expenses, particularly when computing their derivatives. Integrating strain smoothing into IGA has the potential to eliminate the need for costly NURBS function derivatives, thereby enhancing computational efficiency. Furthermore, the using of S-IGA models can lead to enhanced solution accuracy and convergence rates. This improvement can make a big difference, especially in areas like shell structures, where IGA is commonly used.

DongDong et al. [7] proposed a strain smoothing approach for NURBS-based Isogeometric finite element analysis. However, this study differs in method and explores three distinct models: varying cell-based, node-based, and edge-based models.

2. Isogeometric Analysis with Strain Smoothing Technique

This section offers an overview of the fundamental theories and essential information necessary for the development of S-IGA models. The methodology described in this chapter is designed to be applicable to all S-IGA models. Here, the focus lies on implementing and testing S-IGA models for static and stable two-dimensional problems. Consider a 2D solid mechanics problem domain Ω, bounded by Neumann boundary Γ^N and Dirichlet boundary Γ^D, such that $\Gamma^N \cup \Gamma^D = \Gamma$ and $\Gamma^N \cap \Gamma^D = \emptyset$, The proposed S-IGA numerical scheme operates as follows:

2.1. Smoothing Domain Creation

The process of creating smoothing domains for S-IGA models begins by discretizing the domain into a number of elements, following the same procedure as in standard IGA, which generates an element mesh. Unlike S-FEM, where models are primarily constructed in physical space, S-IGA models are essentially built in parameter space. This approach is adopted because the parameter space offers a clear

and standardized definition for the domain mesh, specifying the number of elements (N_e), nodes (N_n), and edges (N_{eg}). An innovative approach was developed to accurately map all necessary quantities for implementing the strain smoothing technique in IGA from the parameter space to the physical space. The problem's discretized domain in the parameter space is subsequently partitioned into a collection of "non-overlapping" and "no-gap" smoothing domains, denoted as Ω_k^s. Each smoothing domain typically comprises n_s sub-smoothing domains.

2.1.1. Cell-based Isogeometric Smoothed Analysis (CS-IGA)

The typical approach to constructing CS-IGA models involves partitioning the quadrilateral element in the parameter space into quadrilateral smoothing domains within the element. This subdivision of each element into multiple smoothing domains is achieved by connecting equidistant points on one edge with corresponding points on the opposite edge, as depicted in Figure 1(a) and 1(b).

2.1.2. Node-based Isogeometric Smoothed Analysis (NS-IGA)

This method involves establishing smoothing domains related to element nodes on top of the domain mesh. Consequently, the overall count of smoothing domains equals the total number of nodes, denoted as $N_s = N_n$. To construct the smoothing domain linked with a node k in the parameter space, mid-edge points are sequentially connected to the central points of the neighboring elements of node k, as depicted in Figure 1(c). The smoothing domain associated with node k includes the aggregation of all subdomains from the surrounding elements.

2.1.3. Edge-based Isogeometric Smoothed Analysis (ES-IGA)

In ES-IGA, the smoothing domain is linked to the edge. It is generated in the parameter space for both inner and outer edges by connecting the two endpoints of the edge with the central points of adjacent elements, as illustrated in Figure 1(d). Therefore, the total count of smoothing domains equals the total number of edges ($N_s = N_{eg}$).

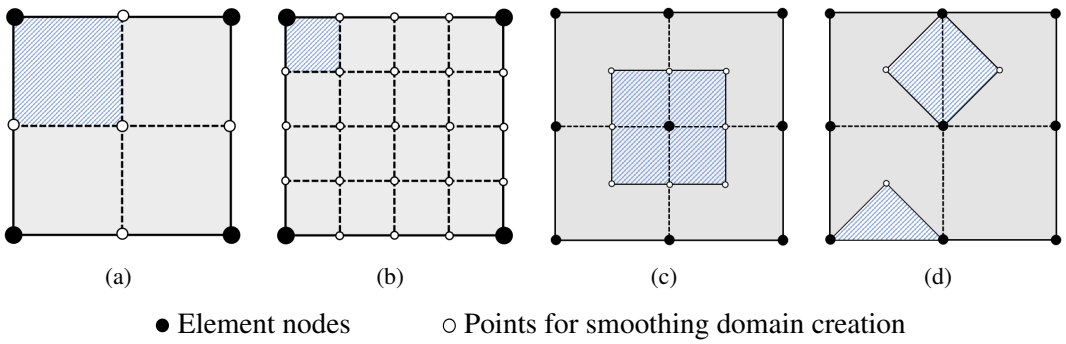

Figure 1: Three techniques for generating smoothing domains in the parameter space:(a) cell-based - 4 smoothing domains; (b) cell-based - 16 smoothing domains; (c) node-based and (d) edge-based

2.2. Values of NURBS Basis Functions

The values of the NURBS basis functions are determined exclusively at locations along the boundaries of the smoothing domains, specifically at the Gauss points intended for integrating the weak form of equilibrium. Unlike in S-FEM models, the calculation of quadratic (or higher-order) NURBS basis function values relies on the Cox-de Boor formula and cannot be obtained through the linear Point Interpolation Method (PIM) (for further information on the PIM, refer to [4]). Additionally, there's no need to compute the derivatives of these basis functions, as is typically done in standard IGA models.

2.3. Smoothed Strain Field Construction

The smoothed strain field in S-IGA models is derived using the strain smoothing technique employed in S-FEM models, under two key assumptions outlined by Liu [4]. First, within the smoothing domain, the strain is estimated by smoothing the compatible strain field. Second, the smoothed strain field is assumed to remain constant throughout the entire smoothing domain.

Equation 1 represents the smoothed strain equation for the S-IGA model, which is the same equation derived for the S-FEM model in [4].

$$\bar{\varepsilon}(x) = \sum_{I=1}^{n_{cp}} \bar{B}_I(x)\bar{d}_I = \begin{bmatrix} \bar{B}_1(x) & \bar{B}_2(x) & ... & \bar{B}_{N_{cp}}(x) \end{bmatrix} \bar{d} = \bar{B}(x)\bar{d}, \tag{1}$$

where B represents the global "smoothed strain-displacement" matrix and n_{cp} denotes the total number of control points in the system. The Matrix $\bar{B}_I(x)$ exhibits non-zero values only for the group of control points supporting the smoothing domain containing x. This set consists all supporting control points of elements contributing to the respective smoothing domain. The computation of $\bar{B}_I(x)$ can be performed, as outlined in Equations 3, following the approach introduced by Liu et al. [4].

$$\bar{B}_I(x) = \frac{1}{A_k^s}\int_{\Gamma_k^s} L_n(x)R_I(x)d\Gamma = \begin{bmatrix} \bar{b}_{Ix} & 0 \\ 0 & \bar{b}_{Iy} \\ \bar{b}_{Iy} & \bar{b}_{Ix} \end{bmatrix}, \bar{b}_{Ih} = \frac{1}{A_k^s}\int_{\Gamma_k^s} n_k(x)R_I(x)d\Gamma, \quad h = x, y. \tag{2}$$

The integration across the smoothing domain boundary employs the Gauss quadrature rule. Specifically, one Gauss point is applied for the line integration along each segment $\Gamma_{k,p}^s$ of boundary Γ_k^s, as depicted in Figure 2. However, due to the non-linear nature of the displacement field along the boundary Γ_k^s, employing multiple Gauss points per segment provides a more accurate approximation. Converting the integration presented in Equation 2 for $\bar{b}_{Ih}$ into a summation yields:

$$\bar{b}_{Ih} = \frac{1}{A_k^s}\sum_{p=1}^{n_\Gamma^s} n_{h,p}R_I(x_p^G)l_p, \quad h = x, y, \tag{3}$$

Here, A_k^s represents the area of the smoothing domain in physical space, and n_Γ^s denotes the total number of boundary segments $\Gamma_{k,p}^s$ within the smoothing domain boundary Γ_k^s. The coordinates of the Gauss

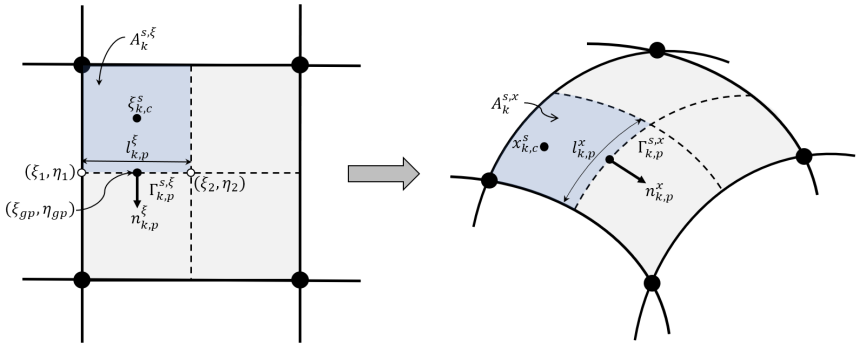

(a) (b)

Figure 2: Mapping of smoothing domains quantities from (a) parametric space to (b) physical space.

point located at the midpoint of the boundary segment $\Gamma^s_{k,p}$ are denoted by x^G_p. Additionally, the length of $\Gamma^s_{k,p}$ and the outward unit normal vector at its midpoint are represented by l_p and $n_{h,p}$, respectively. The values of smoothing domain area (A^s_k), edges lengths (l_p), and normal vectors (n_p) at Gauss points in physical space are determined by mapping the equivalent quantities from the parametric space, as illustrated in Figure 2. This mapping necessitates the computation of the Jacobian matrix at the center of the smoothing domain in the parameter space ($J_{k,c}$). The transformation relations described in Equation 4 are employed to convert line and area values from parametric space to physical space, similar to the role of a deformation gradient in transforming elements from their reference configuration to their deformed configuration. Importantly, this mapping remains valid regardless of the shape of elements in the physical space. For elements with linear edges, these quantities can be easily computed using straightforward mathematical operations.

$$\begin{cases} A^{s,x}_k & = detJ_{k,c} \cdot A^{s,\xi}_k \\ l^x_{k,p} & = \sum_{I=1}^{2} \left\| J^T_{k,c} \cdot \left[(\xi_I - \xi_{gp}) \quad (\eta_I - \eta_{gp}) \right]^T \right\|, \\ n^x_{k,p} & = J^{-1}_{k,c} \cdot n^{\xi}_{k,p} \end{cases} \tag{4}$$

The determinant of the Jacobian matrix calculated at the center point of the smoothing domain is denoted as $detJ_{k,c}$, while $A^{s,\xi}k$ represents the area of the smoothing domain in parameter space. The parametric coordinates of the start and end points of edge p are given as (ξ_I, η_I) with $I = 1, 2$, and $(\xi gp, \eta_{gp})$ represent the coordinates of the Gauss point for edge $\Gamma^{s,\xi}k, p$. The vector $n^{\xi}k, p$ includes the components of the unit outward normal vector calculated at the Gauss point in parameter space.

2.4. Discretizing and Solving the Linear Algebraic System of Equations

After obtaining the smoothed strain displacement matrix, the sub-stiffness matrix for control point I with respect to J is calculated. Next, the stiffness matrix is computed for each smoothing domain and assembled into the global stiffness matrix $\bar{K}$. Upon completion of the assembly, Dirichlet boundary conditions are enforced to restrict all rigid body movements and eliminate singularity. Using this reduced stiffness matrix and the load vector, displacements at the control points are determined through the equation $\bar{\mathbf{K}}\bar{\mathbf{d}} = \bar{\mathbf{f}}$. Once displacements are obtained, the displacement field for the entire domain can be established. Subsequently, strains and stresses are computed during post-processing using the strain-displacement and constitutive relations, respectively.

2.5. Error Assessment in IGA and S-IGA

To assess the outcomes of the S-IGA models, a comparison will be made with both the standard IGA and analytical solutions using displacement and energy norms. Stress values at element nodes will also be compared against analytical solutions. However, evaluating strains and stresses at element nodes in S-IGA is not as straightforward as in IGA. Initially, average strain values are computed for each smoothing domain ($\bar{\varepsilon}^s_k$), and then strains/stresses at node j are determined as area-weighted averages of the surrounding smoothing domains, calculated using Equation 5. Here, n^j_s represents the number of smoothing domains around node j, A^{ns}_j is the total area of all smoothing domains around node j, $\bar{\varepsilon}^s_k$ is the smoothing strain of smoothing domain k, and A^s_k denotes the area of smoothing domain k.

$$\bar{\varepsilon}_j = \frac{1}{A^{ns}_j} \sum_{k=1}^{n^j_s} \bar{\varepsilon}^s_k A^s_k, \tag{5}$$

3. S-IGA for Structural Mechanics Problems

To evaluate the efficacy of the proposed method, the performance of S-IGA models will be assessed against standard IGA solutions in terms of accuracy, convergence rate, and efficiency. This evaluation will be conducted using select structural mechanics problems with known analytical solutions. Two specific examples will be examined: a cantilever beam subjected to parabolic loading at the free end and a hollow disk under inner pressure. Each problem will be analyzed using four numerical models: IGA, 4CS-IGA, NS-IGA, and ES-IGA. These models utilize quadratic NURBS functions for both geometric representation and numerical solution in both directions. Boundary conditions will be modeled using only Dirichlet boundary conditions, imposing exact known displacements on all domain boundaries. This approach helps eliminate errors that may arise from modeling Neumann boundary conditions.

3.1. Numerical Examples: Cantilever Beam

The first benchmark problem under investigation is the rectangular cantilever beam, depicted in Figure 3. In this scenario, the beam experiences a maximum parabolic vertical traction of $P = 1000$ along its free edge, with the assumption of a plane stress condition. The geometric and material parameters are defined as follows: beam length $L = 48$, beam height $H = 12$, modulus of elasticity $E = 3 \times 10^7$, moment of inertia $I = H^3/12 = 144$, and Poisson's ratio $\nu = 0.3$. The analytical solution is given in Equation 6 by reference [8]. The cantilever beam domain is discretized into three regular meshes of 4-sided elements with dimensions (8×2), (16×4), and (32×8).

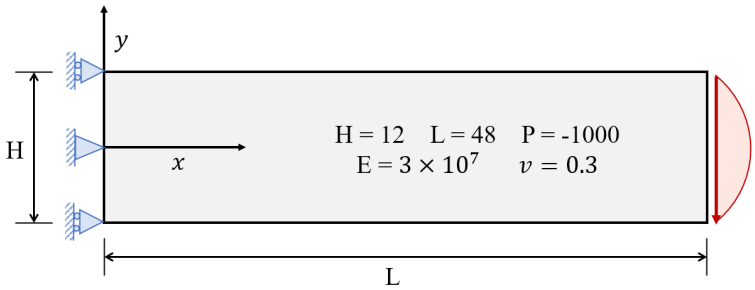

Figure 3: Rectangular cantilever beam with a parabolic load at the free end

$$\begin{cases} u_x(x,y) = \dfrac{Py}{6EI}\left[(6L-3x)x + (2+v)\left(y^2 - \dfrac{H^2}{4}\right)\right] \\ u_y(x,y) = -\dfrac{P}{6EI}\left[3vy^2(L-x) + (4+5v)\dfrac{H^2x}{4} + (3L-x)x^2\right] \\ \sigma_{xx}(x,y) = \dfrac{P(L-x)y}{I}, \qquad \sigma_{yy}(x,y) = 0, \qquad \tau_{xy}(x,y) = -\dfrac{P}{2I}\left(\dfrac{H^2}{4} - y^2\right) \end{cases}, \tag{6}$$

The displacement and energy norms of S-IGA models are compared with those of IGA model in Figure 4 (a) and (b). The ES-IGA model shows noticeably better performance in terms of displacement norm error compared to the standard IGA model. The convergence rate and accuracy in the displacement norm of the IGA, CS-IGA, and NS-IGA models are nearly identical (almost the same). Regarding the energy norm, the standard IGA exhibits the smallest error with the best convergence rate.

Figure 4 (c) and (d) compares the computational time of various numerical methods for achieving solutions of equivalent accuracy. The ES-IGA model emerges as the clear winner in terms of efficiency when measured by the displacement norm, closely followed by the 4CS-IGA model in second place. Both of these methods deliver accurate solutions akin to the standard IGA but within a shorter computational

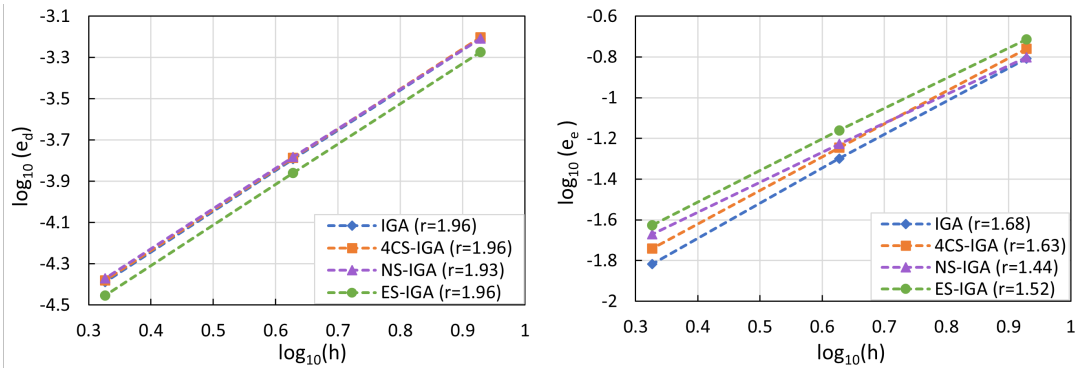

(a) Errors in displacement norm (b) Errors in energy norm

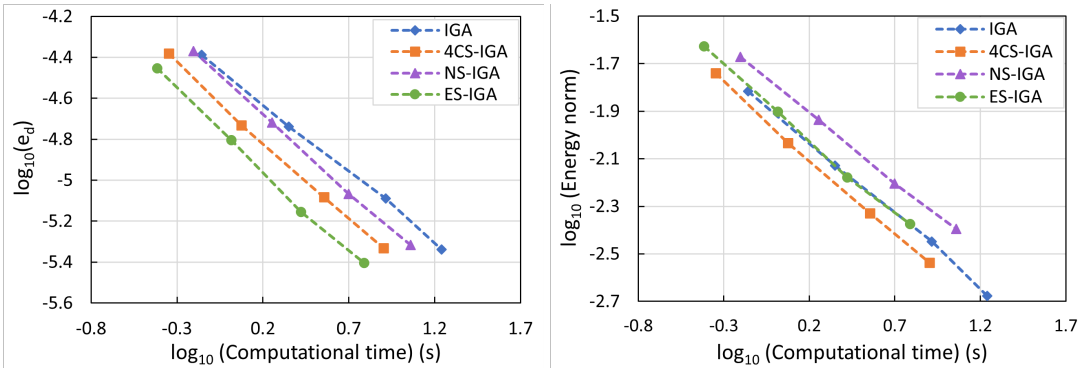

(c) Efficiency in displacement norm (d) Efficiency in energy norm

Figure 4: Errors and efficiencies of IGA and S-IGA models for the cantilever beam problem in displacement and energy norms.

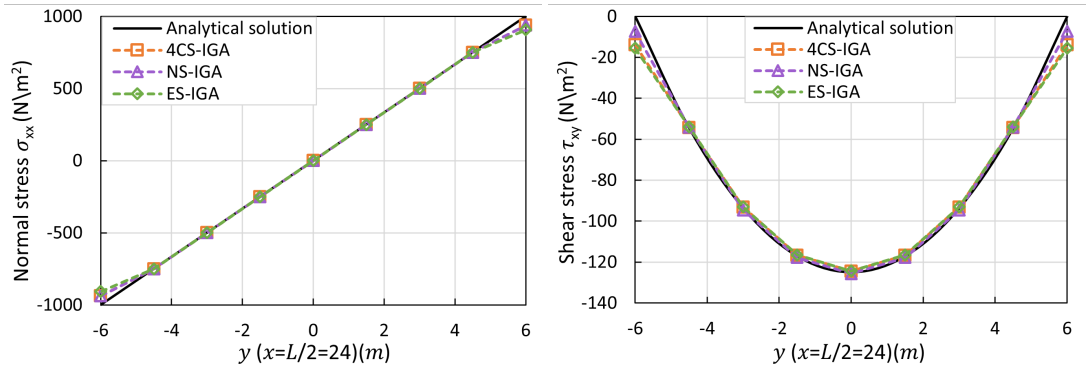

(a) (b)

Figure 5: Exact and numerical stresses in the cantilever beam problem using 4CS-IGA, NS-IGA and ES-IGA models (a) σ_{xx} and (b) τ_{xy}

time. However, in terms of efficiency measured by the energy norm, the 4CS-IGA model excels as the top performer, while the ES-IGA model is deemed equally efficient as the standard IGA.

Figures 5 present a comparison between normal and shear stresses computed at the nodes with the analytical solution. The smoothed numerical solutions closely match the exact solution away from the

problem boundaries. However, the accuracy of stress solutions near the boundaries is slightly diminished compared to those in the inner regions. This phenomenon has also been observed and discussed by Liu et al. [4, 9, 10], who attribute it to the non-symmetry of smoothing domain creation at the boundaries.

3.2. Numerical Examples: Hollow Disk

Another problem investigated in this study is the elastic hollow disk problem, as depicted in Figure 6. To facilitate numerical analysis, only a quarter portion of the disk is modeled due to its symmetry. The disk is subjected to an internal pressure of magnitude $P = 1$, and a plane stress condition is assumed. The geometric and material properties include an outer radius of $b = 5$, inner radius of $a = 1$, modulus of elasticity of $E = 1$, and Poisson's ratio of $\nu = 0.3$. The analytical displacement and stress solutions given in Equation 7 can be found in [8]. The hollow disk domain is created and divided into three regular meshes comprising 4-sided elements with dimensions (4×4), (8×8), and (16×16). These meshes utilize quadratic NURBS basis functions in both circumferential and radial directions.

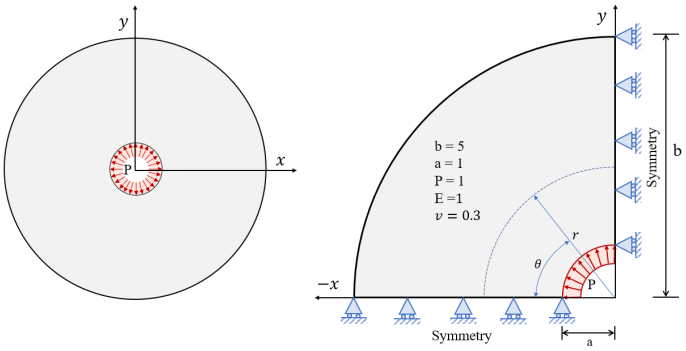

(a) (b)

Figure 6: Elastic hollow disk problem. (a) Problem definition; (b) Numerical model

$$\begin{cases} u_r(r,\theta) = \dfrac{a^2 Pr}{E(b^2-a^2)}\left[1-\nu+\dfrac{b^2}{r^2}(1+\nu)\right], \qquad u_\theta(r,\theta) = 0 \\ \sigma_{rr}(r) = \dfrac{Pa^2}{b^2-a^2} - \dfrac{Pa^2b^2}{r^2(b^2-a^2)}, \qquad \sigma_{\theta\theta}(r) = \dfrac{Pa^2}{b^2-a^2} + \dfrac{Pa^2b^2}{r^2(b^2-a^2)} \end{cases} \tag{7}$$

The displacement and energy norms of both IGA and S-IGA models for the disk with a circular hole problem are illustrated in Figures 7 (a) and (b). It can be observed that, once more, the ES-IGA model yields the smallest error in the displacement norm and an adequately small error in the energy norm. Furthermore, all tested numerical methods, except for the NS-IGA, exhibit roughly the same convergence rate in the displacement norm, approximately 2.

The efficiency comparisons, based on achieving the same accuracy in displacement and energy norms, are illustrated in Figure 7 (c) and (d). Notably, the ES-IGA model emerges as the most efficient solution in terms of displacement norm, requiring only half the time of IGA and three-fifths of the time of 4CS-IGA to achieve the same level of accuracy. Following closely behind, the 4CS-IGA method proves to be the second most efficient approach in displacement norm, demanding approximately two-thirds of the time required by IGA for equivalent accuracy. In terms of energy norm efficiency, the ES-IGA model once again demonstrates its superiority by providing the fastest accurate solution while reducing the computational cost by approximately one-fifth of that required by IGA. Furthermore, when using coarse meshes (i.e., element lengths greater than half), it is observed that 4CS-IGA offers a more efficient

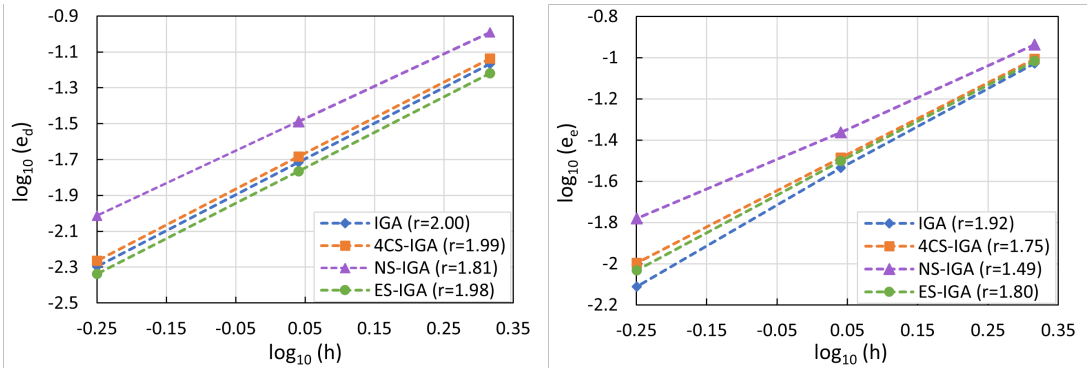

(a) Error in displacement norm

(b) Error in energy norm

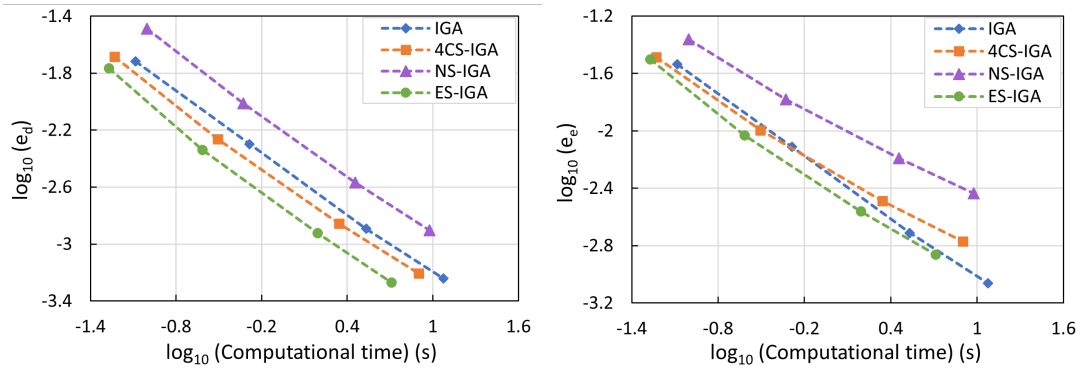

(c) Efficiency in displacement norm

(d) Efficiency in energy norm

Figure 7: Errors and efficiencies of IGA and S-IGA models for the hollow disk problem in displacement and energy norms.

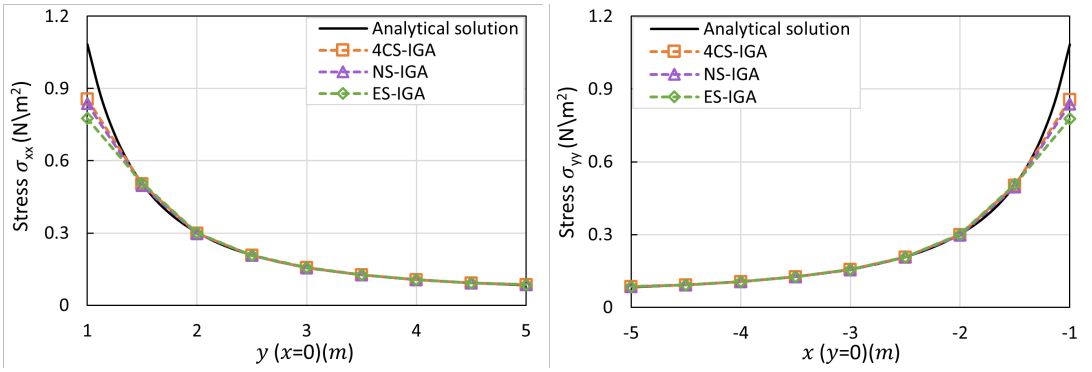

(a) Stress σ_{xx}

(b) Stress σ_{yy}

Figure 8: Exact and numerical stresses of the disk with hole problem using 4CS-IGA, NS-IGA and ES-IGA models (8×8 mesh).

solution than IGA. However, standard IGA's high convergence rate gives it an edge over other S-IGA models, especially with finer meshes. The stresses computed in both the x and y directions using S-IGA models are depicted in Figure 8. Notably, these computed stresses closely match the analytical solution beyond the hole boundary.

4. Conclusion and Outlook

The application of strain smoothing techniques to isogeometric analysis (IGA) has been explored. Three variants of smoothed IGA (S-IGA) models, including cell-based (CS-IGA), node-based (NS-IGA), and edge-based (ES-IGA) models, were investigated. Methodology development and comparison against analytical solutions led to several key findings: S-IGA models maintain computational efficiency by retaining the same number of degrees of freedom as IGA. However, interpolating basis function values along smoothing domain boundaries in S-IGA models necessitates more sophisticated methods due to the nature of quadratic or higher-order functions. Notably, the accuracy and efficiency of ES-IGA and 4CS-IGA models outperform standard IGA, particularly in terms of displacement norm. On a positive note, ES-IGA and 4CS-IGA models often demonstrate high convergence rates in both displacement and energy norms. Nevertheless, stress solutions near problem boundaries in S-IGA models may be less accurate due to asymmetry in smoothing domains.Further exploring strain smoothing techniques in standard IGA holds potential for advancement. This involves investigating their use with triangular elements, which might improve accuracy and computational efficiency. Adapting existing smoothed finite element methods for 3D problems to IGA could also enhance solutions. Additionally, optimizing methods by using multiple Gauss points per edge, increasing smoothing domains for CS-IGA models, and incorporating new basis function types may lead to better numerical schemes.

References

[1] "The finite element method: Its basis and fundamentals," in *The Finite Element Method: its Basis and Fundamentals (Seventh Edition)*, O. Zienkiewicz, R. Taylor, and J. Zhu, Eds., Seventh Edition, Oxford: Butterworth-Heinemann, 2013, p. iii, ISBN: 978-1-85617-633-0.

[2] W. Zeng and G. Liu, "Smoothed finite element methods (s-fem): An overview and recent developments," *Archives of Computational Methods in Engineering*, vol. 25, no. 2, pp. 397–435, 2018.

[3] V. Agrawal and S. S. Gautam, "Iga: A simplified introduction and implementation details for finite element users," *Journal of The Institution of Engineers (India): Series C*, vol. 100, no. 3, pp. 561–585, 2019.

[4] G.-R. Liu and N. Trung, *Smoothed finite element methods*. CRC press, 2016.

[5] T. J. Hughes, J. A. Cottrell, and Y. Bazilevs, "Isogeometric analysis: Cad, finite elements, nurbs, exact geometry and mesh refinement," *Computer methods in applied mechanics and engineering*, vol. 194, no. 39-41, pp. 4135–4195, 2005.

[6] J. A. Cottrell, T. J. Hughes, and Y. Bazilevs, *Isogeometric analysis: toward integration of CAD and FEA*. John Wiley & Sons, 2009.

[7] D. Wang, H. Zhang, and J. Xuan, "A strain smoothing formulation for nurbs-based isogeometric finite element analysis," *Science China Physics, Mechanics and Astronomy*, vol. 55, no. 1, pp. 132–140, 2012.

[8] S. Timoshenko and J. Goodier, *Theory of elasticity 3rd ed., 567*, 1970.

[9] G.-R. Liu and M. B. Liu, *Smoothed particle hydrodynamics: a meshfree particle method*. World scientific, 2003.

[10] J. W. Yoo, B. Moran, and J.-S. Chen, "Stabilized conforming nodal integration in the natural-element method," *International Journal for Numerical Methods in Engineering*, vol. 60, no. 5, pp. 861–890, 2004.